Materials Letters 291 (2021) 129583

Contents lists available at ScienceDirect

Materials Letters

journal homepage: www.elsevier.com/locate/mlblue

Dual-band solar-blind UV photodetectors based on AlGaN/AlN superlattices

Yiren Chen [a,*], Xingyu Zhou [a,b], Zhiwei Zhang [a], Guoqing Miao [a], Hong Jiang [a], Zhiming Li [a], Hang Song [a,*]

[a] State Key Laboratory of Luminescence and Applications, Changchun Institute of Optics, Fine Mechanics and Physics, Chinese Academy of Sciences, Changchun 130033, China
[b] University of Chinese Academy of Sciences, Beijing 100039, China

ARTICLE INFO

Article history:
Received 30 January 2021
Received in revised form 17 February 2021
Accepted 17 February 2021
Available online 23 February 2021

Keywords:
Epitaxial growth
Sensors
Dual-band
Solar-blind ultraviolet
AlGaN/AlN superlattices
MOCVD

ABSTRACT

Herein, a metal–semiconductor-metal (MSM) structure dual-band solar-blind ultraviolet (UV) photodetector based on 60.5-period $Al_{0.5}Ga_{0.5}N$/AlN superlattices (SLs) is reported. The device exhibits distinct dominant responses in the solar-blind UV region with dual peaks located at 266 nm and 243 nm. The formation of dual-band solar-blind UV photodetection is clarified, which can be originated from the reflection enhancement property of the highly periodic $Al_{0.5}Ga_{0.5}N$/AlN SLs that restrains the light absorption around 259 nm resulting in weak spectral response in this specific waveband.

1. Introduction

Due to its tunable direct bandgap ranging from 3.4 eV (GaN) to 6.2 eV (AlN), aluminum gallium nitride (AlGaN) material has been considered to be one of the core materials for the development of deep ultraviolet (DUV) optoelectronic devices, e.g., DUV light-emitting diodes (LEDs) [1,2], laser diodes (LDs) [3], and solar-blind photodetectors (SB-PDs) [4,5]. Among them, AlGaN-based SB-PDs have extensive application and market prospects in the fields of ultra-high voltage (UHV) power grids for their corona leakage detection, important military and civil targets protection against missile approaching threat, and chemical/biological agent inspection for public biosecurity as well [6]. In order to enhance the target recognition ability of AlGaN-based SB-PDs to adapt to the increasingly complex target environment, the traditional single detection band determined by the inherent optical bandgap of AlGaN material is unable to meet the practical application requirements. Therefore, the realization of dual- or even multi-band detection on a single absorber material has drawn great attention nowadays. However, it is an enormous challenge to fulfill distinctive spectral detection on a single absorber material with a specific bandgap (E_g), especially in the solar-blind UV region. In the past decade, Sandvik et al. demonstrated dual SiC-based photodiodes for simultaneous two-band UV detection [7]. Xie et al. realized solar-blind and visible-blind double wavelength photodetection on a single mixed-phased MgZnO detector on the basis of Mg content variation caused by phase segregation [8]. Gökkavas et al. fabricated dual spectral responsivity bands (including solar-blind and visible-blind) on a single $Al_xGa_{1-x}N$ heterostructure accomplished by the incorporation and removal of an *in-situ* epitaxial AlGaN filter layer [9]. Although some studies have reported on the dual-band UV photodetection using a single semiconductor, there is still limited research on this topic in the solar-blind UV region.

In this letter, a MSM structure solar-blind UV photodetector with high sensitivity based on AlGaN/AlN superlattices (SLs) is fabricated, which presents dual-channel photodetection in the solar-blind UV region. The mechanism involved in the formation of dual-band is also clarified, which can be ascribed to the reflection property of the periodic superlattices at a specific waveband that inhibits the light absorption.

2. Experimental procedure

The epitaxial growth was implemented on a 2-inch c-plane sapphire substrate by a high-temperature MOCVD (HT-MOCVD) equipped with an *in-situ* optical monitoring system (LayTec AG). The metal–semiconductor-metal (MSM) structure photodetector was fabricated by the standard lift-off process. A scanning electron

* Corresponding authors.
E-mail addresses: chenyr@ciomp.ac.cn (Y. Chen), songh@ciomp.ac.cn (H. Song).

https://doi.org/10.1016/j.matlet.2021.129583
0167-577X/

microscope (SEM, Hitachi S4800) was used to characterize the cross-sectional image of the $Al_{0.5}Ga_{0.5}N$/AlN superlattices (SLs). The symmetrical and asymmetrical reciprocal space mapping (RSM) images around (0 0 0 2) and (1 0 $\bar{1}$ 5) reflections for the material were characterized by a high-resolution X-ray diffractometer (HRXRD, Bruker D8). A spectrograph equipped with a 50 mW 213 nm-wavelength Nd:YAG deep UV laser (Advanced Optowave) as the excitation source was used to obtain the Photoluminescence (PL) spectrum. The reflection spectrum of the epitaxial material was measured by a UV–Vis-NIR spectrophotometer (PerkinElmer Lambda 900) at room-temperature. The electrical characteristics of the photodetector were obtained by a sourcemeter (Keithley 237) and its spectral response properties were measured by a silicon-based standard detector calibrated UV spectral response tester equipped with a 300 W xenon lamp.

3. Results and discussion

Fig. 1(a) presents the *in-situ* monitoring curves of reflectance by 405-nm-wavelength and emissivity-corrected temperature for the epitaxial material, which is composed of a 700 nm-thick AlN layer and a 60.5-period $Al_{0.5}Ga_{0.5}N$/AlN SLs layer (inset of Fig. 1(b)). The former AlN layer is epitaxially grown by the method of introducing a mesothermal (MT-AlN) interlayer and regulating the growth rate of high-temperature AlN (HT-AlN) on its both sides based on the conventional two-step growth method. For detailed growth process, it can be referred to in our previous report [5]. The latter SLs layer is prepared on the AlN layer by periodically supplying additional trimethylgallium (TMGa) source along with the continual supply of trimethylaluminium (TMAl) and ammonia (NH_3), under the conditions of 1200 °C and 50 mbar chamber pressure. Fig. 1(b) shows the cross-sectional SEM image of the epitaxial material, in which the 60.5-period $Al_{0.5}Ga_{0.5}N$/AlN SLs present a clear layered stack with a constant periodic thickness distribution. The thickness of one period of $Al_{0.5}Ga_{0.5}N$/AlN is roughly estimated as 20 nm/22 nm, as shown in the partial enlarged image of Fig. 1 (b). The optical property of the 60.5-period $Al_{0.5}Ga_{0.5}N$/AlN SLs is investigated by room-temperature PL, which exhibits a strong near-band-edge emission around 280 nm (~4.42 eV) assuming a small Stokes shift compared with the theoretical bandgap of $Al_{0.5}Ga_{0.5}N$ (~4.55 eV) [10].

The typical reciprocal space mapping (RSM) images for the epitaxial material around the (0 0 0 2) and (1 0 $\bar{1}$ 5) reflections measured by HRXRD are shown in Fig. 2(a) and (b). A series of well-resolved superlattice fringes originated from the periodic $Al_{0.5}Ga_{0.5}N$/AlN bistratal structure are clearly observed in the symmetric RSM around (0 0 0 2) reflection. Inset of Fig. 2(a) shows its (0 0 0 2) plane 2θ-ω scanning curve. Besides the characteristic diffraction peak of the AlN (red arrow), high-order satellite peaks indicate the $Al_{0.5}Ga_{0.5}N$/AlN SLs exhibit a good periodicity and abrupt interfaces, as illustrated in SEM image. In Fig. 2(b), the RSM around (1 0 $\bar{1}$ 5) reflection presents a series of superlattice fringes in addition to a well-resolved main peak corresponding to the AlN. The reciprocal lattice point (RLP) denoted as ($\boldsymbol{q_x}$, $\boldsymbol{q_z}$) for AlN in Fig. 2(b) is evaluated as (-3.071, 10.037), which is in accordance with that of the full relaxed bulk AlN [11], indicating the strain-free of the AlN template. The high-order superlattice fringes distributed along the $\boldsymbol{q_z}$ axis (guided by the black dashed line) have the same $\boldsymbol{q_x}$, indicating that the whole $Al_{0.5}Ga_{0.5}N$/AlN SLs layer has the same in-plane lattice parameter. This means that it coherently grows on AlN layer regardless of the lattice mismatch between $Al_{0.5}Ga_{0.5}N$ and AlN.

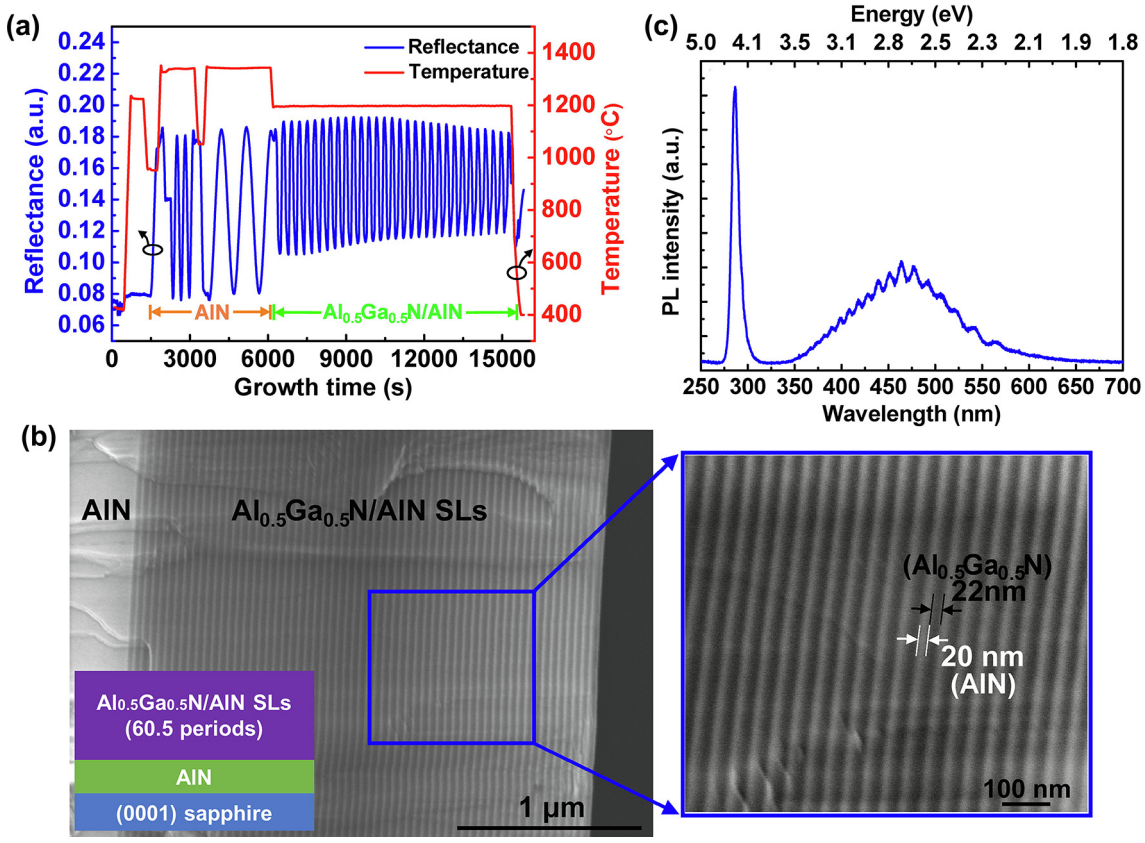

Fig. 1. (a) Transients of reflectance and emissivity-corrected temperature for the epitaxial material. (b) The cross-sectional image of the $Al_{0.5}Ga_{0.5}N$/AlN SLs and its partial enlarged structure. Inset shows the structural diagram of the epilayers. (c) The PL spectrum of the $Al_{0.5}Ga_{0.5}N$/AlN SLs.

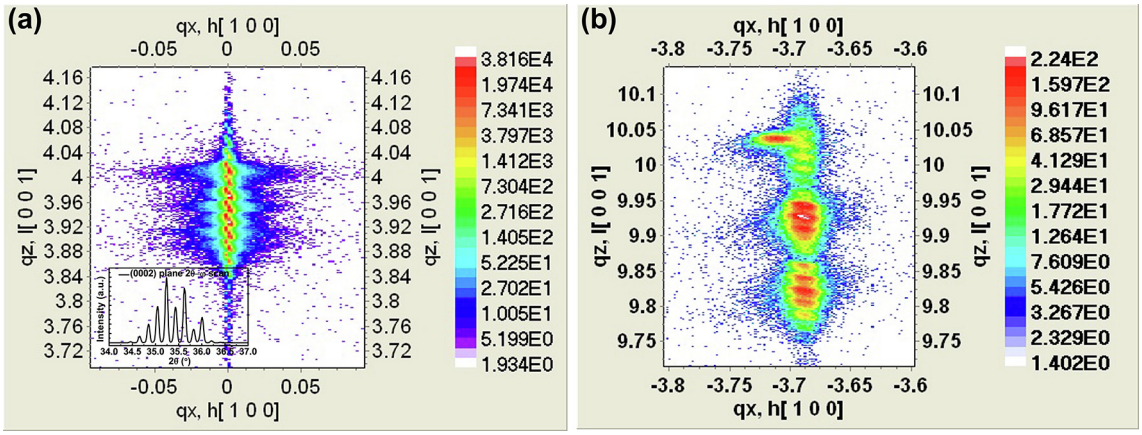

Fig. 2. The typical RSM images for the epitaxial material (a) around (0002) plane and (b) around (10-15) plane.

Based on the 60.5-period $Al_{0.5}Ga_{0.5}N$/AlN SLs, a MSM structure photodetector consisting of 50 sets of Ni/Au (30 nm/200 nm) interdigital electrodes is fabricated by standard photolithography, electron-beam evaporation and lift-off processes [12]. Fig. 3(a) and (b) show the schematic configuration and the physical image of the fabricated MSM structure photodetector, respectively. The interdigital finger is 10 μm-width, 100 μm-length separated by 10 μm. In order to investigate the performance of the device, the electrical properties are firstly measured. Fig. 3(c) presents its current–voltage (*I-V*) curves in dark and under the illumination of 270-nm-wavelength light. By contrast, the ratio of the photocurrent to the dark current is at least two orders of magnitude under different bias voltages. The measured spectral responsivities and the corresponding external quantum efficiencies (EQEs) under different biases are presented in Fig. 3(d) and inset. As can be seen, the bias-dependent response spectra exhibit dual-band feature in the solar-blind UV wavelength with one peak located at 266 nm and the other at 243 nm. The responsivity and corresponding EQE of peak located at 266 nm increase from 52.6 mA/W and 24.5% at zero-bias to 190.7 mA/W and 89.3% at 100 V while those of peak located at 243 nm increase from 29.2 mA/W and 14.8% to 130.5 mA/W and 66.6%.

In order to explain the formation of dual-band in the solar-blind UV region, the reflection spectrum of the 60.5-pair $Al_{0.5}Ga_{0.5}N$/AlN SLs is measured, as shown in Fig. 3(e). The reflection spectrum in the solar-blind UV band presents the characteristics of decreased reflection around 269 nm (red dashed line of inset) and enhanced reflection around 259 nm (blue dashed line of inset) with clear interference fringes at the long-wavelength direction. The wavelengths of the red and blue dashed lines in Fig. 3(e) correspond to those of the red and blue dashed lines on the spectral response curves in Fig. 3(d). It is intuitively found that the weak reflection region (around red dashed lines) corresponds to the high spectral responsivity while the strong reflection region (around blue

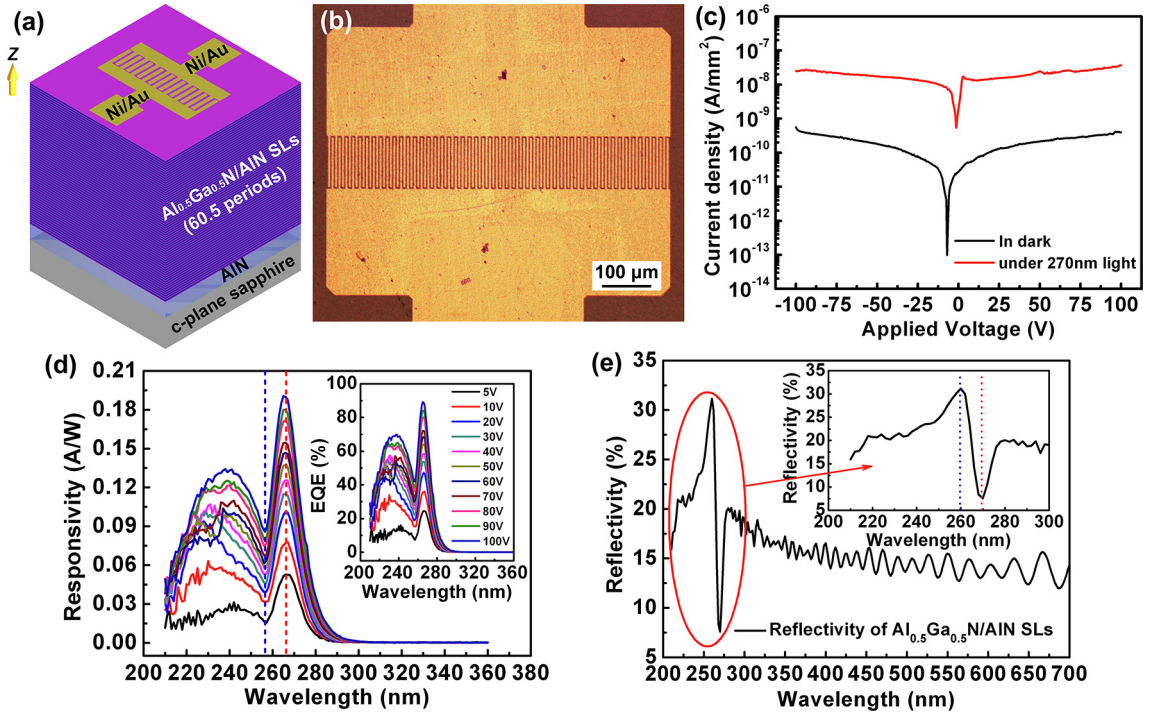

Fig. 3. (a) The schematic configuration of a MSM structure photodetector based on $Al_{0.5}Ga_{0.5}N$/AlN SLs and (b) its physical image. (c) The electrical properties of the photodetector in dark and under 270 nm-wavelength illumination. (d) The measured spectral responsivities under different biases. Inset shows the corresponding EQEs. (e) Reflection spectrum for 60.5-pair $Al_{0.5}Ga_{0.5}N$/AlN SLs.

dashed line) to the low spectral responsivity. This implies that the enhanced reflection around 259 nm inhibits the light absorption and thus weakens the spectral responsivity of the photodetector, which leads to the formation of dual-channel in the solar-blind UV region. It should be noted that the wavelengths of the red and blue dashed lines in Fig. 3(d) have a slight blue shift, which can be attributed to the band deformation of SLs caused by the applied bias during spectral response test.

4. Conclusions

In summary, a 60.5-period $Al_{0.5}Ga_{0.5}N$/AlN SLs layer with high periodicity and abrupt interfaces is epitaxially grown by HT-MOCVD. Based on the SLs, a MSM structure photodetector is fabricated and characterized, which presents dual-band photodetection in the solar-blind UV region with dual peaks located at 266 nm and 243 nm. The responsivities for both peaks are 190.7 mA/W and 130.5 mA/W at 100 V, corresponding to an EQE of 89.3% and 66.6%, respectively. The mechanism involved in the formation of dual-band photodetection can be attributed to the reflection enhancement property of the periodic $Al_{0.5}Ga_{0.5}N$/AlN SLs around 259 nm that inhibits the light absorption, and thus results in the weak spectral response in this region.

CRediT authorship contribution statement

Yiren Chen: Conceptualization, Methodology, Data curation, Writing - original draft, Funding acquisition. **Xingyu Zhou:** Data curation, Writing - original draft. **Zhiwei Zhang:** Methodology, Investigation. **Guoqing Miao:** Validation, Resources. **Hong Jiang:** Project administration, Resources. **Zhiming Li:** Investigation, Visualization. **Hang Song:** Supervision, Writing - review & editing, Funding acquisition.

Declaration of Competing Interest

The authors declare that they have no known competing financial interests or personal relationships that could have appeared to influence the work reported in this paper.

Acknowledgments

This work was supported by National Natural Science Foundation of China (Grant Nos. 61504144 and 51472230), and Department of Science and Technology of Jilin Province (Grant No. 20170520156JH).

References

[1] P. Coulon, G. Kusch, R.W. Martin, P.A. Shields, ACS Appl. Mater. Interfaces 10 (2018) 33441–33449.
[2] S. Inoue, N. Tamari, M. Taniguchi, Appl. Phys. Lett. 110 (2017) 141106.
[3] X. Li, H. Xie, F.A. Ponce, J. Ryou, et al., Appl. Phys. Lett. 107 (2015) 241109.
[4] A. Kalra, S. Rathkanthiwar, R. Muralidharan, S. Raghavan, et al., IEEE Photon. Technol. Lett. 31 (2019) 1237–1240.
[5] Y. Chen, Z. Zhang, G. Miao, H. Jiang, et al., Mater. Lett. 281 (2020) 128638.
[6] T.A. Growden, W. Zhang, E.R. Brown, D.F. Storm, et al., Light Sci. Appl. 7 (2018) 17150.
[7] P. Sandvik, D. Brown, J. Fedison, K. Matocha, et al., J. Electrochem. Soc. 152 (2005) G199.
[8] X.H. Xie, Z.Z. Zhang, C.X. Shan, H.Y. Chen, et al., Appl. Phys. Lett. 101 (2012) 081104.
[9] M. Gökkavas, S. Butun, H. Yu, T. Tut, et al., Appl. Phys. Lett. 89 (2006) 143503.
[10] A. Franke, M.P. Hoffmann, L. Hernandez-Balderrama, F. Kaess, et al., Proc. SPIE 9748 (2016) 97481G.
[11] Y. Chen, Z. Zhang, H. Jiang, Z. Li, et al., J. Mater. Chem. C 6 (2018) 4936–4942.
[12] S. Rathkanthiwar, A. Kalra, S.V. Solanke, N. Mohta, et al., J. Appl. Phys. 121 (2017) 164502.